Myosin-IIA and ICAM-1 Regulate the Interchange between Two Distinct Modes of T Cell Migration[1]

Jordan Jacobelli, F. Chris Bennett, Priya Pandurangi, Aaron J. Tooley, and Matthew F. Krummel[2]

How T cells achieve rapid chemotactic motility under certain circumstances and efficient cell surface surveillance in others is not fully understood. We show that T lymphocytes are motile in two distinct modes: a fast "amoeboid-like" mode, which uses sequential discontinuous contacts to the substrate; and a slower mode using a single continuously translating adhesion, similar to mesenchymal motility. Myosin-IIA is necessary for fast amoeboid motility, and our data suggests that this occurs via cyclical rear-mediated compressions that eliminate existing adhesions while licensing subsequent ones at the front of the cell. Regulation of Myosin-IIA function in T cells is thus a key mechanism to regulate surface contact area and crawling velocity within different environments. This can provide T lymphocytes with motile and adhesive properties that are uniquely suited toward alternative requirements for immune surveillance and response. *The Journal of Immunology,* **2009, 182: 2041–2050.**

Cellular migration is a key process for development, morphogenesis, wound healing, and immune responses and depends upon an interplay of actin polymerization and myosin-dependent compression and retraction (1–3). In large adherent cells, crawling occurs during cycles of leading edge extensions in the lamellipod, generation of adhesion sites beneath the lamella, and disengagement from the substrate at the rear (2, 3). This generates a continuously translating adhesion zone beneath the motile cell. Although many of the general principles gleaned from fibroblasts and epithelial cells might apply to "fast" (5–20 μm/min) amoeboid-like cells, such as T lymphocytes and neutrophils, the specific mechanisms of actomyosin function that underlie the interplay between motility and adherence in T cells are less clear (4, 5). Differences are expected both on the basis of their specialized functions and characteristic amoeboid shape, as well as the absence of demonstrated focal adhesions and lack of tissue remodeling during their migration (4, 6). Furthermore, it is likely that, in vivo, different migration strategies and mechanisms are used based on the specific environment a lymphocyte encounters (for example during transendothelial migration vs crawling within lymph nodes) (7, 8). An example of switching migration strategy has been reported in the case of tumor cells, which can convert from a mesenchymal to an amoeboid motility mode following metalloproteinase inhibition (9, 10). In addition, studies in the amoeba *Dictyostelium* (11) and in neutrophils (12) have suggested the possibility of motility kinetics with discontinuous adhesion characteristics, but the causes and molecular details remain unknown. Given the number of T cell functions that rely on migration to specific tissues and interaction with other cells (8, 13), we sought to examine the general principles of motility in lymphocytes, particularly in relation to substrate adhesion and motility modes.

Nonmuscle myosin-II is thought to provide the primary force for contraction of actin filaments during motility. However, the actual role of myosin-II in regulating migration of adherent cells such as fibroblasts and epithelial cells is somewhat unclear. Inhibition of myosin-II has been reported to result in either the reduction (14, 15) or the enhancement of cell migration (16). In addition, different isoforms of myosin-II may play opposing roles in the migration of specific cell types (17). In contrast, in amoeboid cells such as *Dictyostelium*, myosin-II has been shown to positively regulate cell migration (18, 19). In addition, in T cells, myosin-II appears to alter adhesions and inhibition of this motor on ICAM-1-rich substrates has been reported to inhibit trailing edge retraction (20, 21). Moreover, myosin-II-deficient *Dictyostelium*, which lacks integrins, also shows enhanced adhesion (22, 23). We have previously reported that myosin-IIA (MyoIIA, NMMHC-IIA, *MyH9*) is the only class-II myosin isoform expressed in murine T cells and that this myosin is a key component for motility of T cells in a two-dimensional environment (24).

Materials and Methods

Cells

The D10.G4 $CD4^+$ T cell clone (D10) was cultured in RPMI 1640 medium supplemented with 10% FBS and 5 U/ml IL-2. D10 cells were restimulated weekly with feeder $I\text{-}A^k$ MHC splenocytes and cognate Ag (conalbumin peptide 134–146). D10 T cells were split 3 days after Ag restimulation and every 2 days thereafter; cells were used for experiments at least 7 days after Ag restimulation. Activated primary T cells were derived from DO.11.10 TCR transgenic mice (on a BALB/c background), purchased from The Jackson Laboratory; cells were used 5 or 6 days after stimulation with congenic splenocytes pulsed with OVA peptide (323–333). All mice were bred and maintained in accordance with the guidelines of the Laboratory Animal Resource Center of the University of California at San Francisco. The imaging medium used was complete RPMI 1640 without phenol red, with the addition of 5 U/ml IL-2 and 10 mM HEPES.

Abs and reagents

Rabbit polyclonal anti-class II Myosin (BTI) was used for immunofluorescence and immunoblotting. FITC-conjugated anti-rabbit secondary Ab

Department of Pathology, University of California San Francisco, San Francisco CA 94143

Received for publication September 30, 2008. Accepted for publication December 8, 2008.

The costs of publication of this article were defrayed in part by the payment of page charges. This article must therefore be hereby marked *advertisement* in accordance with 18 U.S.C. Section 1734 solely to indicate this fact.

[1] This work was supported by National Institutes of Health (R01AI052116) and the Leukemia and Lymphoma Society (to M.F.K.).

[2] Address correspondence and reprint requests to Dr. Matthew F. Krummel, Department of Pathology, University of California San Francisco, 513 Parnassus Avenue, San Francisco CA 94143. E-mail address: matthew.krummel@ucsf.edu

www.jimmunol.org/cgi/doi/10.4049/jimmunol.0803267

was purchased from Jackson Immunoresearch Laboratories. Rhodamine-conjugated phalloidin was from Invitrogen. Mouse monoclonal anti-tubulin, aprotinin, leupeptin, PMSF, sodium fluoride, iodoacetamide, and sodium orthovanadate were purchased from Sigma-Aldrich. HRP-conjugated protein A and detergent-compatible protein assay kit, were purchased from Bio-Rad. Blebbistatin (racemic mix) was from Calbiochem and was used at 100 μM. Casein (Sigma-Aldrich) and ICAM-1-Fc (R&D Systems) were used to coat glass chamberslides (Nalge Nunc International) at a concentration of 80 nM for 1 h at 37°C. Bovine collagen I was purchased from R&D Systems.

Short-hairpin RNA vector construction and transfection

The short hairpin RNA (shRNA)[3] plasmid pSilencer 2.0-U6 was purchased from Ambion. Hairpin shRNA primers were designed with *Bam*HI and *Hind*III overhangs for cloning as described in the pSilencer manual. The sequence of the MyoIIA-6592 shRNA was: TCCGACTGTAAACCGTCT CAA; and the MyoIIA-7075 shRNA was: CTGTGATTAGGTTCCCTTA; both sequences target the 3′-UTR of the MyoIIA (*MyH9*) mRNA. The control shRNA sequence was: ACTACCGTTGTTATAGGAG. shRNA plasmids were electroporated (300 V and 975 μF capacitance) in D10 T cells together with a GFP-expressing plasmid or an actin-GFP plasmid at a 5:1 molar ratio for selection and imaging purposes. Forty-eight hours after transfection, GFP-positive cells were sorted and used for experiments 24 h after sorting. Given that MyoIIA-6592 shRNA construct gave the best knockdown and inhibition of T cell velocity it was selected for use in our experiments.

Fluorescent protein plasmid transfection for microscopy

MyoIIA heavy chain (*MyH9*) was cloned by PCR from cDNA obtained from murine primary T cells and inserted in the GFP-C1 vector from Clontech. To create the actin-mCherry plasmid, we swapped mCherry (a gift of R. Tsien, University of California San Diego, La Jolla, CA) into an actin-GFP vector obtained from B. Imoff (University Medical Centre, Geneva, Switzerland). The actin and myosin plasmids were coelectroporated at a 1:1 molar ratio as described above. Transfected cells were sorted for MyoIIA-GFP$^+$ and actin-mCherry$^+$ cells 24 h after electroporation. Expression of MyoIIA-GFP in our imaging experiments resulted in an average overexpression of only 30–50% relative to the endogenous protein as assessed by intracellular FACS and/or Western blotting. This overexpression of MyoIIA-GFP did not change the overall frequencies of walking vs sliding: on control surfaces "walking" frequency was 92%, while on ICAM-1 "walking" frequency dropped to 15%. These results are comparable to the frequencies obtained in cells not transfected with MyoIIA-GFP (shown in Fig. 2*e*).

Immunoblotting

Immunoblotting was routinely performed as described in (24) to quantify the level of MyoIIA knockdown. MyoIIA shRNA no. 6592 achieved a knockdown of 65–80% while MyoIIA shRNA no. 7075 knockdown was 45–55%. Tubulin immunoblotting was performed as a control to normalize MyoIIA knockdown densitometry.

Migration assays

Migration in collagen lattices was performed by mixing a 1.5× collagen solution 2:1 with activated primary T cells resuspended at 2×10^6/ml in RPMI 1640 with 20% FCS, 20 U of IL-2, and 20 mM HEPES, and labeled with 2 μM (5(and-6)-(((4-chloro-methyl)benzoyl)amino)tetramethylrhodamine (CMTMR) (Invitrogen). When used, blebbistatin was present at a final "in-lattice" concentration of 100 μM. After 1 h incubation at 37°C to let the collagen fully polymerize the cells were imaged by confocal microscopy acquiring 50 μm deep Z-stacks of the collagen lattice every 30 s for 30 min.

Migration assays on two-dimensional surfaces were performed by plating 5×10^4 D10 T cells in glass chamberslides and adding low melting-point agarose to a final concentration of 0.1%, cells were then left overnight at 37°C and imaged the next morning. For shRNA knockdown experiments, brightfield and GFP images were acquired at 15 s intervals for 20 min.

For analysis, cell viability was assessed using the brightfield images while cell movement was measured based on the center of mass of GFP or CMTMR fluorescence using Imaris tracking software (Bitplane). Cells that did not have a displacement grater than 10 μm (~1 cell length) were scored as nonmotile. For migration experiments involving blebbistatin, cells were labeled with CMTMR and imaging and analysis was performed as described above. CMTMR (excited at 541–569 nm) was used to avoid exposure of blebbistatin-treated cells to light at <500 nm to prevent photoinactivation and toxicity of blebbistatin (25).

Microscope setup

Widefield imaging for migration assays was performed on a modified Axiovert 200M microscope (Zeiss) with a 20×/0.75 NA objective and a Coolsnap HQ camera (Roper Scientific). Confocal imaging was done using a modified Axiovert 200M microscope equipped with a spinning-disk confocal scanner (Yokogawa) with a 40×/1.3 NA oil immersion objective and an iXon EMCCD camera from Andor. Total internal reflection fluorescence (TIRF) imaging was performed on a modified Axiovert 200M microscope fitted with a Zeiss TIRF slider and a 100×/1.45 NA oil immersion objective. The Widefield and Confocal microscopes were equipped with dual excitation and emission filter wheels and the control and imaging software was Metamorph (Universal Imaging Corp.). TIRF images were acquired with a liquid-cooled intensified CCD camera (model XR/Mega-10Z) from Stanford Photonics. The TIRF microscope was equipped with 491 nm (50mW) and 561 nm (25 mW) solid-state lasers (Cobolt); excitation wavelength was selected through an acousto-optical tunable filter. Emission wavelengths were selected through the combination of a multiple-edge dichroic and multiple-pass emission filter. The control and imaging software was InVivo (QED Imaging/Media Cybernetics). All microscopes were configured with heated stages to maintain sample temperature at 37°C.

TIRF microscopy

For TIRF imaging of contact zones, 5×10^4 cells were plated overnight in chamberslides with the addition of 0.1% low melting point agarose to increase the viscosity of the medium. Brightfield and TIRF fluorescence images were acquired for each wavelength every 2 s for 5 or 10 min depending on the experiment. TIRF imaging involving the use of blebbistatin-treated cells was performed using actin-mCherry as a marker of contact zones and exciting the cells with 561 nm laser light to avoid blebbistatin toxicity as described above.

Data analysis

Contact zone measurement was performed using Metamorph software, actin-GFP fluorescence was thresholded, and the area of the fluorescent region was then calculated using the "region statistics" function of Metamorph. Determination of the crawling mode was performed using the "stack arithmetic" function of Metamorph to average over time the thresholded actin-GFP fluorescence of the contact zones (detected in the TIRF field) for the duration of a timelapse. If the time-averaged rendition showed only one main contact zone the cell was scored as "sliding," if multiple distinct contact zones were present the cell was scored as "walking." In timelapse experiments, a cell with multiple contact zones was scored as "mixed" if it presented a single contact zone for more than half of the duration of a timelapse.

Kymograph analysis for Fig. 5 was performed using Metamorph, the fluorescence intensities of myosin-GFP and actin-mCherry were calculated for each point on a 5 pixel-wide line along the path of the cell during a timelapse (traced by tracking the center-of-mass of the contact zone/s).

For the analysis of the relative distribution of myosin and actin in crawling T cells, first the actin contact zones were thresholded and the area of these zones was calculated for the entire timelapse using the "graph intensities" function. The ratio of MyoIIA to actin fluorescence intensity in the thresholded areas was calculated by dividing the myosin fluorescence values by the actin fluorescence values and multiplying the result by 100; this value is shown as relative MyoIIA intensity (in arbitrary units) in the graphs of Fig. 5. If distinct contact zones were present (i.e., in the "walking" mode), each parameter was calculated separately for every contact zone.

To compare the acto-myosin behavior in the two motility modes, in walking cells, MyoIIA contractions were scored as "full" if a local maximum in the myosin/actin ratio preceding the appearance of a new contact zone reached a peak of at least 2-fold the average initial "baseline" level of the ratio. If the ratio only reached 1.5-fold, the average initial level or the appearance of a new contact zone was delayed (>60 s) relative to the peak of the myosin/actin ratio the myosin contraction was scored as "partial." Finally, if no local maximum in the myosin/actin ratio of at least 1.5-fold the initial baseline value was reached, the contraction was scored as "none."

The movement and speed of MyoIIA clusters within a contact area were analyzed using National Institutes of Health Image and the MTrackJ plugin. Myosin clusters from timelapse sequences were first highlighted using a "convolving" filter and then the clusters were manually tracked using the "bright centroid" recognition function of MTrackJ.

[3] Abbreviations used in this paper: shRNA, short hairpin RNA; TIRF, total internal reflection fluorescence; CMTMR, (5(and-6)-(((4-chloro-methyl)benzoyl)amino)-tetramethylrhodamine.

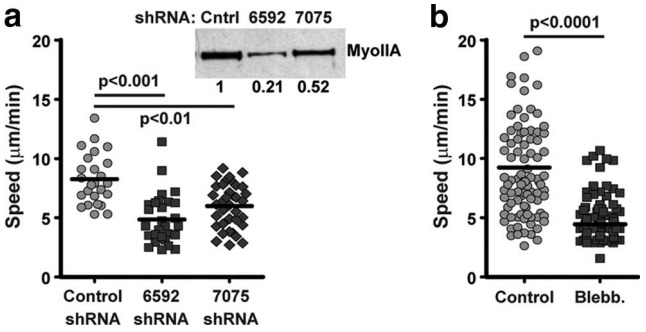

FIGURE 1. Comparison of shRNA vs chemical inhibition of MyoIIA. *a*, Average crawling speed of sorted control-shRNA or MyoIIA-shRNA treated D10 T cells 72 h after transfection. Two shRNAs directed against distinct regions of the MyoIIA mRNA 3′ UTR with consistent knockdown of 65–80% (MyoIIA construct no. 6592) and of 45–55% (MyoIIA construct no. 7075) were used, resulting in an average reduction of velocity of 41 and 27%, respectively. The MyoIIA-6592 shRNA construct resulted in the best knockdown and inhibition of T cell velocity and was therefore selected for use in our additional experiments. *Inset* panel shows Western blot and quantification of MyoIIA knockdown. *b*, Average crawling speeds of vehicle control or 100 μM blebbistatin treated D10 T cells after 1 h of incubation. Results are representative of three independent experiments.

Statistical analysis

Continuous variable data was analyzed first by determining whether it was normally distributed and had equal variance, in which case ANOVA for multiple comparisons, followed by post hoc Tukey tests, or Student's *t* test, for single comparisons, were performed to determine statistical significance. Alternatively, for non-normally distributed data, Kruskal-Wallis or Mann-Whitney tests were used to determine statistical significance followed by Dunn post tests to determine *p* values for multiple comparisons. Nominal variable data was analyzed using the Chi-square test to determine significance.

Results

MyoIIA is necessary for a discontinuous crawling mode

Given the limited information on the interplay between adhesion and acto-myosin contractility during lymphocyte motility we sought to study the mechanistic role of MyoIIA in regulating T cell surface-contacts where force is generated in connection with motility rate. To analyze the fine molecular details of these force-generating contacts during motility, we adopted a TIRF microscopy-based approach in concert with shRNA-mediated knockdown of MyoIIA. TIRF microscopy allows for direct assessment of contact-site molecular dynamics at high resolution. Although use of shRNA, instead of the class-II myosin chemical inhibitor blebbistatin (26), to inhibit MyoIIA function permits the use of GFP and other fluorophores whose illumination would otherwise adversely affect cells in the presence of blebbistatin (25). In addition, while blebbistatin treatment initially induced a nearly complete arrest (during which cells can continue to produce leading-edge extensions; Ref. 24), over the next 30 min, T cells partially recover motility to a rate up to 48% of the vehicle control, just below that seen with the MyoIIA shRNAs (Fig. 1, *a* and *b*). The initial and more dramatic arrest may be a consequence of the acute loss of cellular tension induced by inhibition of MyoIIA motor function or a result of additional targets of blebbistatin.

We used actin-GFP to visualize the contact zones by TIRF illumination; this imaging technique limits the detection of fluorescent signals to ~100 nm above the coverslip, effectively highlighting the F- or G- actin at cellular adhesion sites on the substrate without exciting fluorophores in noncontacting regions or in the cytoplasm above.

We tracked T cells during motility on defined adhesion surfaces in the presence or absence of MyoIIA expression. Whereas fibroblasts and epithelial cells migrate using an adhesion zone that grows from the front and contracts at the rear (2), T cells on low adhesion strength surfaces did not typically display this mechanism of motility. Rather, T cell amoeboid motility was frequently characterized by a series of sequential and spatially distinct contact zones with the substrate (Fig. 2*a* and supplemental movie 1).[4] The formation of each new contact occurred forward along the direction of cell migration in close temporal proximity with the contraction of the previous adhesion. We called this motility mode "walking" as the cells appeared to generate sequential adhesive footprints as an integral part of the crawling process. The dynamic nature of these multiple distinct contact zones was highlighted by averaging over time the actin-GFP fluorescence in the TIRF field for the duration of the timelapse sequence of a crawling cell (Fig. 2*a*, *right panel*). This analysis showed the existence of distinct contact zones which progress in the general direction of cell travel and which are typically poorly physically connected to one another during walking.

Conversely, in MyoIIA-depleted T cells, we observed an adhesion pattern that more closely resembled that reported for fibroblasts and epithelial cells: a single contact zone that progressively extended at the front and retracted at the rear (Fig. 2*b* and supplemental movie 2). We called this second motility mode "sliding". This difference in motility mode was not only controlled by MyoIIA levels but also by the nature of the substrate. Analysis of the contact zone dynamics of control cells plated on ICAM-1 showed that, when on a high adhesion strength substrate, T cells typically switched to a sliding mode of crawling regardless of the presence of MyoIIA (Fig. 2, *c* and *d*, and supplemental movies 3 and 4).

Quantification of the frequency of these two crawling modes showed that D10 T cells predominantly used the walking mode when crawling in the absence of LFA-1 ligands and switched to the sliding mode in the presence of ICAM-1 ($p < 0.0001$) (Fig. 2*e*). We also observed a subset of cells that interchanged between modes on either type of substrate (scored as mixed in Fig. 2, *e* and *f*). Regardless of the adhesion strength of the substrate, MyoIIA-depleted T cells crawled almost exclusively using the sliding mode ($p < 0.0001$) (Fig. 2*e*). Motility also switched to the sliding mode of crawling even in the absence of ICAM-1 in the presence of blebbistatin, ($p < 0.0001$) (Fig. 2*f*), further supporting a requirement for MyoIIA for walking amoeboid motility.

Finally, we studied how the two distinct motility modes could affect the overall crawling speed of T cells. In amoeboid D10 T cells, the walking mode correlated, at least in part, with the high motility rate, with walking cells crawling on average 1.6 times faster than sliding cells (Fig. 2*g*). Walking control cells (pooled from cells crawling on either blocked- or ICAM-1-surfaces) crawled at an average speed of 9.5 μm/min, while the average speed of pooled sliding control cells was 5.8 μm/min ($p < 0.001$). Consistent with our previous data, the motility rate and mode strongly correlated with both MyoIIA expression and substrate adhesion strength. Accordingly, most control-shRNA treated cells on low adhesion substrates crawled using a walking motility mode and these cells were faster than MyoIIA depleted cells which predominantly used a sliding mode (Fig. 2*g*). Our findings correlate with the reported phenotype of myosin-II mutant *Dictyostelium* which show greater reduction of motility rates on high-concentration polylysine-coated surfaces vs uncoated or low-concentration polylysine coating (27).

[4] The online version of this article contains supplemental material.

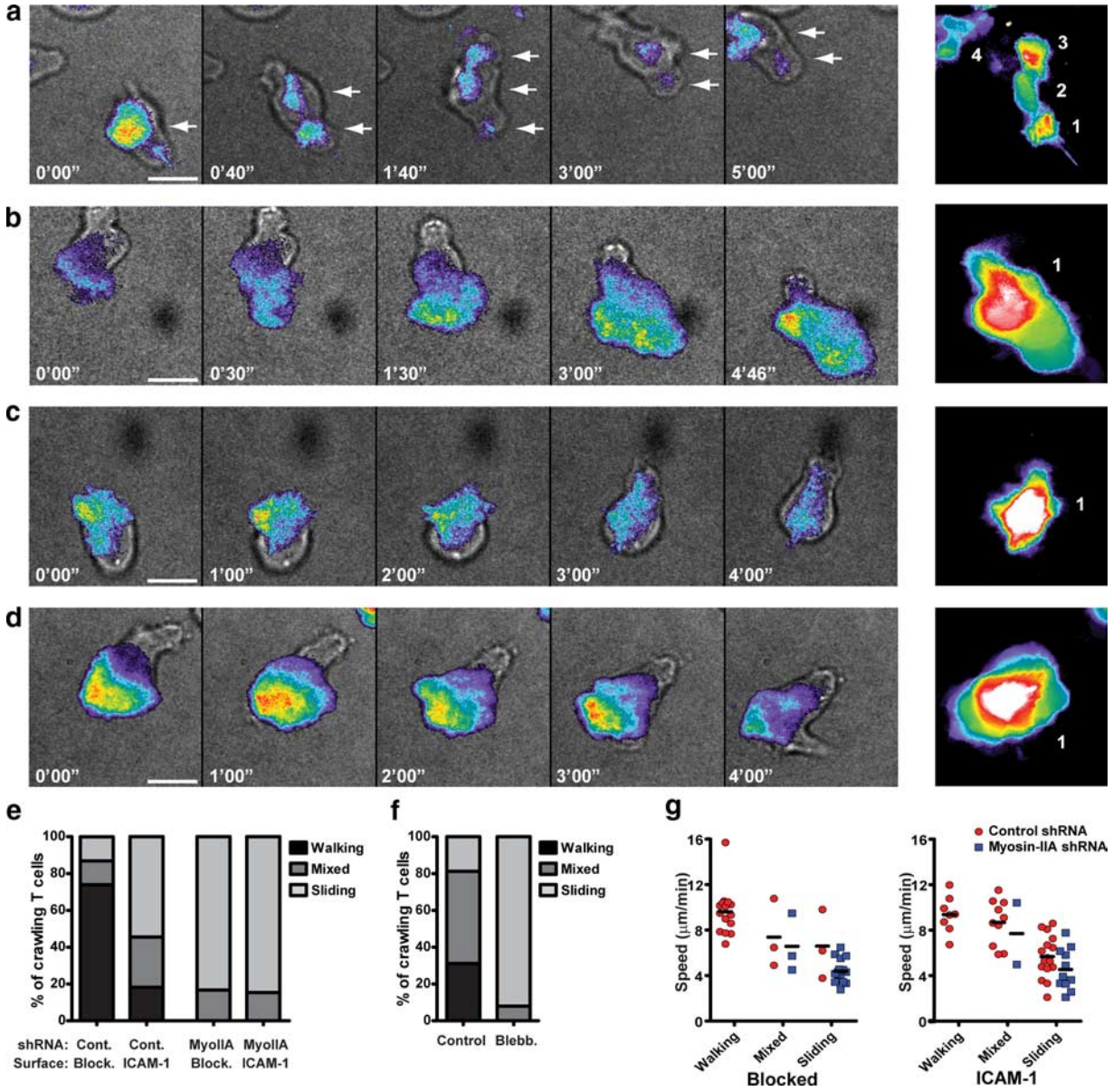

FIGURE 2. MyoIIA levels and substrate adhesion strength regulate two distinct motility modes for T cells. *a*, Representative walking D10 T cell. D10 T cells were cotransfected with control-shRNA and actin-GFP plasmids and then sorted 48 h after transfection and plated in casein blocked chamberslides overnight. Cells were imaged by TIRF microscopy at 2 s intervals for 10 min. Individual timepoints, from left to right, chosen from live imaging timecourses are shown (available as supplemental movie 1). Brightfield images are overlayed with a pseudo-colored TIRF image of the actin-GFP fluorescence. White arrows highlight separate contact zones. Scale bars, 10 μm. *Right panel*, A time-averaged pseudo-color rendering of the actin-GFP contact zones during the timecourses. Numbers indicate the separate contact zones. *b*, Representative sliding D10 T cell. D10 T cells cotransfected with MyoIIA-shRNA, and actin-GFP plasmids were plated in casein-blocked chamberslides and then imaged and analyzed as described above (available as supplemental movie 2). *c*, D10 T cells cotransfected with control-shRNA and actin-GFP plasmids were plated on ICAM-1 coated chamberslides and analyzed as described (available as supplemental movie 3). *d*, D10 T cells cotransfected with MyoIIA-shRNA, and actin-GFP plasmids were plated on ICAM-1 coated chamberslides and analyzed as described (available as supplemental movie 4). *e*, Quantification of D10 T cell crawling modes upon treatment with control- or MyoIIA-shRNA and plating in casein (blocked) or ICAM-1 coated chamberslides (as indicated). Cells were cotransfected with actin-GFP plasmids and imaged as described above. Scoring of migration mode was based on the appearance or lack of multiple contact zones (details in *Materials and Methods*). *f*, Quantification of T cell crawling modes upon treatment with blebbistatin. D10 T cells were transfected with an actin-mCherry plasmid, sorted after 24 h, and plated overnight in casein-blocked chamberslides for imaging. One hour before imaging by TIRF, microscopy cells were treated with vehicle control or 100 μM blebbistatin and imaged and scored as described above. *g*, Correlation of crawling mode and speed in D10 T cells plated on blocked or ICAM-1 surfaces. For each cell, the crawling mode was assessed by analyzing the dynamics of the actin-GFP contact zones while the overall cell speed was quantified based on the brightfield images. Results in *a–f* are representative of three independent experiments. Results in *g* are pooled from three independent experiments.

Analysis of activated primary T cells confirmed that primary amoeboid T cells could exhibit either crawling mode (Fig. 3, *a* and *b*). Our data also showed that, similar to D10 T cells, in primary T cells the adhesion strength of the substrate correlated with the frequency of the two crawling modes and the size of the contact area (Fig. 3, *c* and *d*). Furthermore, analysis of HL-60 neutrophils showed that these amoeboid leukocytes are also able to migrate with two distinct crawling modes (data not shown).

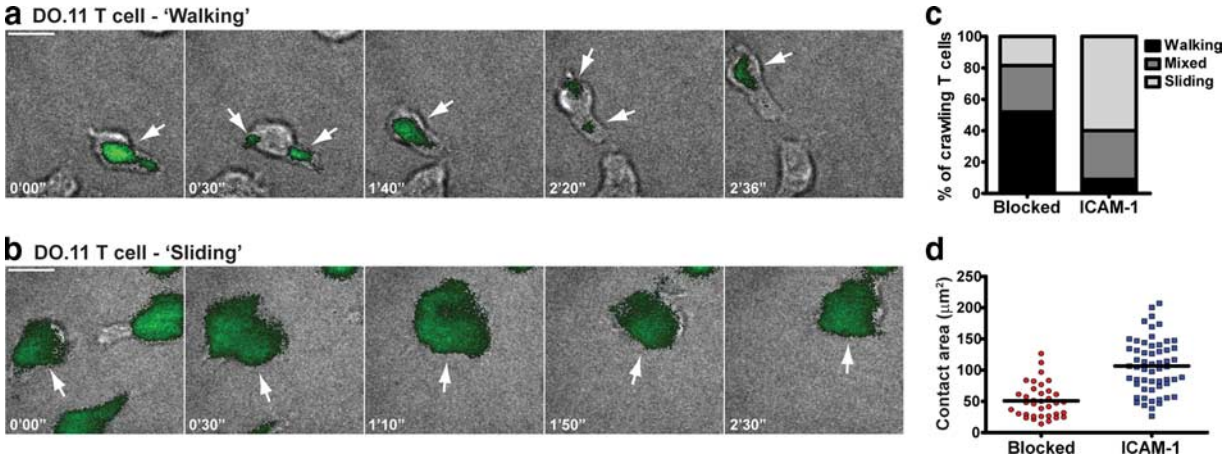

FIGURE 3. Activated primary T cells exhibit dual-crawling modes. Primary DO.11.10 TCR transgenic T cells were used 5 days after activation. T cells were labeled with 0.25 μM CFSE and then plated overnight in chamberslides coated with casein or ICAM-1 and then imaged by TIRF microscopy at 2 s intervals for 5 min. *a*, Representative walking primary T cell crawling on a casein blocked surface. White arrows highlight the contact zones. *b*, Representative sliding primary T cell crawling on ICAM-1. *c*, Frequencies of migration modes in primary T cells. DO.11.10 T cells were treated as described above and scoring of migration mode was based on the appearance of multiple contact zones in the CFSE TIRF fluorescence channel (details in *Materials and Methods*). *d*, Cells were imaged by TIRF microscopy and the size of the contact area with the substrate was measured. Scale bars, 10 μm. Results are representative of two independent experiments.

MyoIIA contractions at rear adhesion sites promote "amoeboid" crawling

Given the dependency of the walking mode on MyoIIA, we sought to determine the spatial relationship between MyoIIA distribution throughout the contact zones and the establishment of new contacts. To do this, we labeled T cells with MyoIIA-GFP (to track MyoIIA densities and distribution) and actin-mCherry (to visualize contact zones). In these experiments, over-expression of MyoIIA-GFP was generally not greater than 50% relative to endogenous levels and did not affect the frequencies of walking vs sliding (data not shown, details in *Materials and Methods*).

Key cyclical features of the walking mode emerged from analyzing MyoIIA-GFP distribution in the contact zones. During formation, contact zones were initially actin-rich and myosin-poor

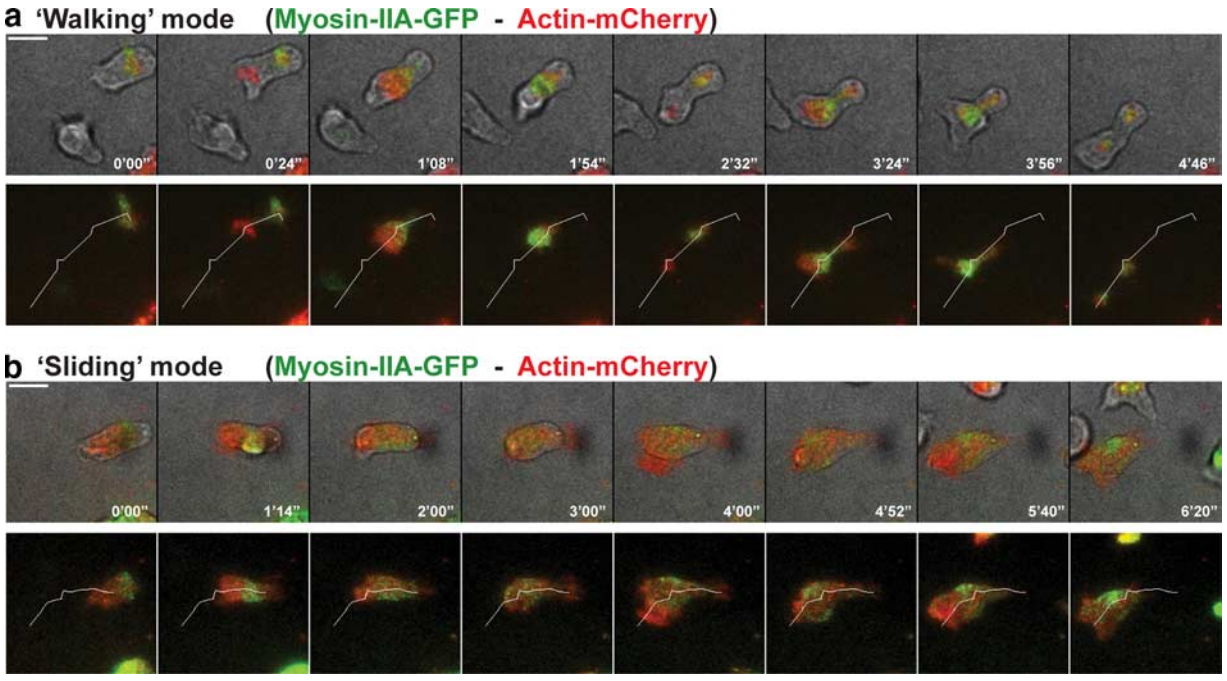

FIGURE 4. MyoIIA and actin dynamics during the two motility modes of T cells. D10 T cells were cotransfected with MyoIIA-GFP and actin-mCherry and sorted for double-positive fluorescent cells 24 h after transfection; cells were then plated overnight in chamberslides for TIRF imaging. *a*, MyoIIA and actin dynamics in a walking cell. Individual timepoints (from *left* to *right*) of a representative walking T cell chosen from live TIRF imaging timecourse experiments (available as supplemental movie 5). The images show the overlay of the MyoIIA-GFP (green) and actin-mCherry (red) fluorescence from the TIRF images on the brightfield image (*upper panel*). The line (based on the cell path) used for the kymograph in Fig. 5 is shown on the overlay of the MyoIIA-GFP and actin-mCherry TIRF images (*lower panel*). *b*, MyoIIA and actin dynamics in a sliding cell. Timepoints from a live imaging timecourse of a representative sliding T cell (available as supplemental movie 6). Images obtained as described in *a*. Scale bars, 10 μm. Data are representative of the average cell behaviors from three independent experiments.

(Fig. 4*a*, 0:24", 2:32" timepoints and supplemental movie 5). Subsequently, MyoIIA was recruited forward into this existing contact zone and became enriched there (Fig. 4*a*, 1:08–1:54" and 3:24–3:56" timepoints). As enrichment proceeded and as the contact zone started to be compressed, new contacts were nucleated at a spot beneath the front of the crawling cell.

In contrast to this, cells using a sliding mode of motility had a single, continuously translating, contact zone that was always relatively rich in actin at its leading edge (Fig. 4*b* and supplemental movie 6). These data suggest that, in both crawling modes expansion at the leading edge of the contact zone, and in walking cells the establishment of new contact zones, may be facilitated by a local absence of MyoIIA. As such, MyoIIA paucity at the leading edge may license these forward membrane domains to form contact zones, likely by releasing cortical tension.

Kymograph analysis of the relative distribution of MyoIIA and actin over time, along a line based on the center of mass of the contact zones during motility, highlighted additional features of the cyclical expansions and contractions of contact zones during crawling (Fig. 5*a*). Most notably, streaks of MyoIIA moved inward, both along and against the direction of motion, as an older contact zone compressed (Fig. 5*a*, highlighted by arrows parallel to the streaks). A strong temporal connection between the recruitment of MyoIIA in the shrinking contact and the appearance of the subsequent one was also evident in the kymographs. In addition, this temporal correlation between the enrichment of MyoIIA at the rear contact zone (Fig. 5*b*, *top*, grayed areas) and appearance of a new contact at the front in the walking mode (Fig. 5*b*, *bottom*, grayed areas) was supported by the quantification of MyoIIA densities in the contact zones over time. Conversely, in the sliding mode MyoIIA intensity remained relatively constant and distinct contact zones were not formed (Fig. 5*d*). Although we commonly observed this difference in MyoIIA dynamics between walking and sliding cells ($p = 0.015$), it was unclear whether there is a strict requirement for a specific degree of MyoIIA enrichment to enable the establishment of a new contact zone. Notably, during crawling, only a fraction of the total MyoIIA was recruited to the contact zones given that MyoIIA-GFP fluorescence remained readily detectable by confocal microscopy throughout the portion of the T cell cortex not in contact with the substrate (data not shown).

Kymographs of cells using sliding motility did not reveal cyclical changes but rather a steady enrichment of actin at the leading edge and forward-moving streaks of MyoIIA (Fig. 5*c*, highlighted by arrows parallel to the streaks), presumably representing forward pulling of the attached cell body along a network of surface-tethered actin. These forward-directed pools of MyoIIA in sliding motility contrast distinctly with the bidirectional movement observed during the elimination of an existing contact zone in the walking mode. Overall, the movement of MyoIIA clusters both forward and rearward relative to center-of-mass movement was a unique feature of walking cells.

We further highlighted the cyclical nature of this process by analyzing the dynamics of expansion and contraction of new contact zones in walking cells. This often appeared to resemble cell spreading, which has elements of radial symmetry, rather than previously studied surface contacts in motility in which spreading and contraction are generally collinear with the direction of motion. Although contact zones grew in all directions, expansion was not symmetric, with a bias toward the front and with a boundary at the rear edge that was not exceeded (Fig. 6*a,* "Expansion", color-coded from gray to black). As suggested by the kymograph analysis, contact zones were often eliminated concentrically during a contraction phase (Fig. 6*a*, "Contraction", color-coded from gray to black). In contrast, sliding cells exhibited a more continuous

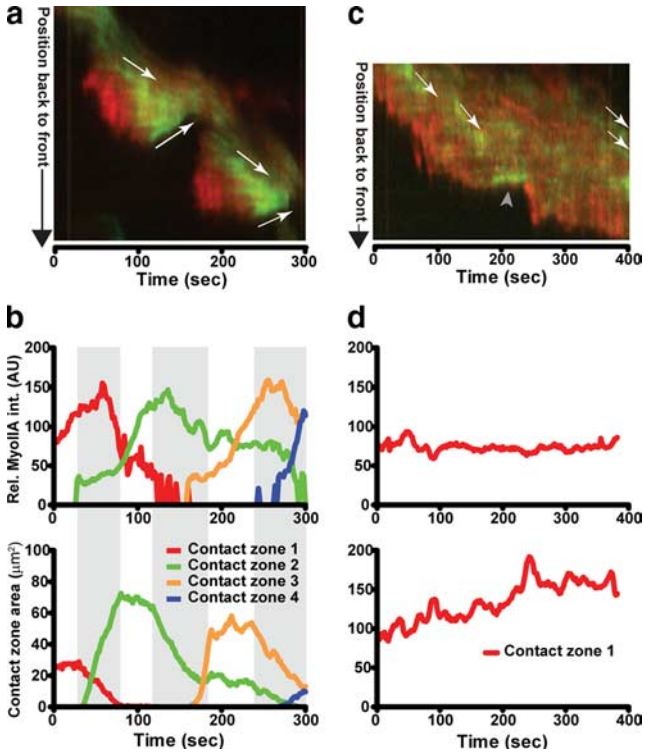

FIGURE 5. MyoIIA promotes the formation of new adhesions through contractions at the existing adhesions. *a*, Kymograph rendition of MyoIIA (green) and actin (red) distribution along the path of migration of the walking cell shown in Fig. 4*a*. The overlay of the fluorescent intensities of MyoIIA-GFP (green) and actin-mCherry (red) is shown for each point along a line following the cell path during the timecourse (further details in *Materials and Methods*). The movement of MyoIIA clusters is highlighted by arrows running parallel to the clusters. *b*, Ratio of MyoIIA-GFP fluorescence intensity relative to that of actin-mCherry (*top panel*) and measurement of the area of each contact zone (*bottom panel*) during the timecourse for the walking cell in Fig. 4*a*. Values for each distinct contact zone were plotted with each subsequent arising contact zone separately numbered and color coded. *c*, Kymograph rendition of the sliding cell shown in Fig. 4*b*. The movement of MyoIIA clusters is highlighted by arrows running parallel to the clusters, while the gray arrowhead indicates a point at which the cell made a turn. Analysis performed as described above. *d*, Ratio of MyoIIA-GFP fluorescence intensity relative to that of actin-mCherry (*top panel*), and measurement of the area of the contact zone (*bottom panel*) for the sliding cell in Fig. 4*b*. Data are representative of the average cell behaviors from three independent experiments.

expansion (at the front) and contraction (at the rear) of the contact zone (Fig. 6*b*, *top panel*). Although leading edge extension was somewhat pulsatile, consistent with a model for spatiotemporal coupling of waves of expansion and retraction at the leading edge during motility (28).

Even though migrating T cells are very dynamic, we were able to track distinct clusters of myosin filaments in close proximity to the membrane as they moved inward during the elimination of contacts in the walking mode. This revealed that individual collections of myosin filaments moved centripetally (Fig. 6, *a* and *c*, *bottom panels*, and supplemental movie 7). This suggested that the plus ends of actin filaments in the contact zones of walking T cells may be oriented away from or toward the center of the contact instead of being aligned in a more linear fashion, although the source of this symmetry remains unclear. Although cluster movements showed elements of spatial symmetry, this was not always temporally uniform. Because these events were not well correlated in time, they suggest that the myosins are not necessarily linked

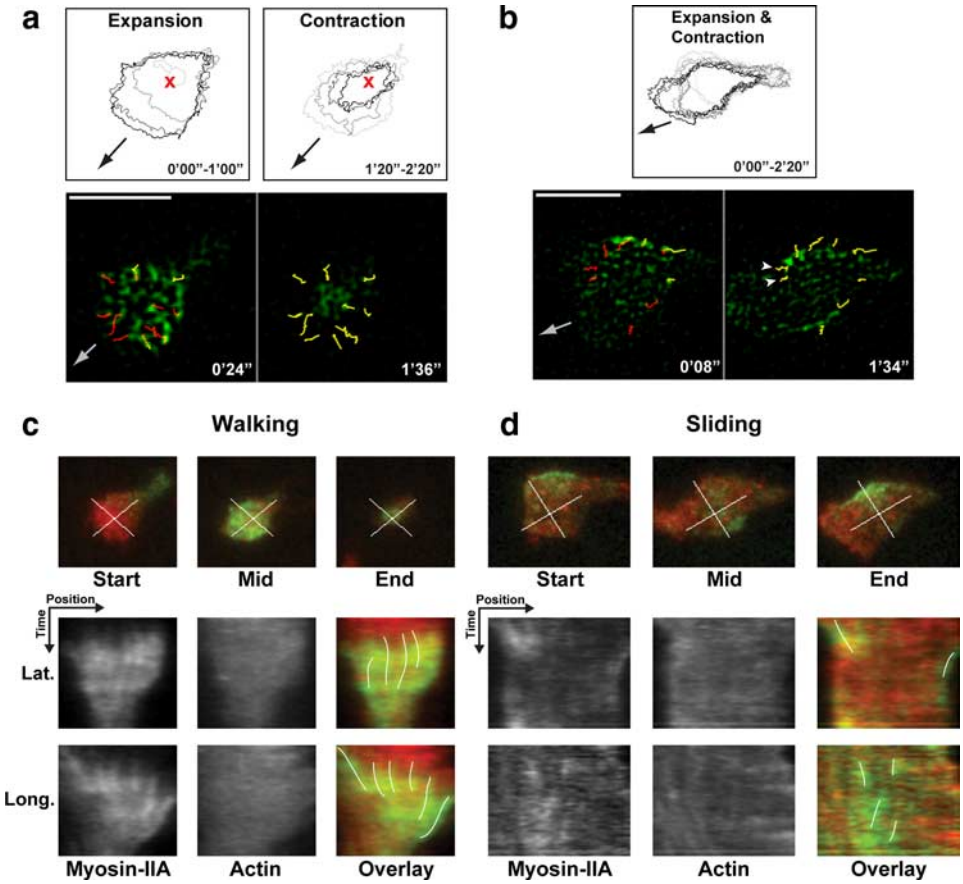

FIGURE 6. MyoIIA cluster coalescence in the adhesion zones of crawling T cells. *a*, *top panels,* Contact zone expansion and contraction in a walking cell. D10 T cells were transfected, treated and imaged as described in Fig. 4. The thresholded outlines of a contact zone were traced at 20 s time intervals, color-coded from gray to black and overlayed to show the contraction and expansion of the contact zone. The expansion and contraction phases (color-coded from gray to black) are shown separately to highlight the distinct phases of the contact zone behavior during walking. The red x is shown as a reference point; the black arrow indicates the general direction of cell migration. *a*, *bottom panels*, Tracking of selected MyoIIA clusters in the contact zone of a walking cell (available as supplemental movie 7). The complete paths of the clusters are overlayed in red, the tracks transition to yellow as each cluster moves along its path. The gray arrow shows the general direction of cell migration. Scale bars, 10 μm. Details in *Materials and Methods. b*, *top panel,* The outlines of a contact zone from a sliding cell are shown. Depicted and analyzed as in *a*. *b*, *bottom panels,* Tracking of selected MyoIIA clusters in the contact zone of a sliding cell (available as supplemental movie 8). White arrowheads highlight MyoIIA clusters that move against the general direction of crawling of the cell. Represented and analyzed as in *a*. *c*, *top panels*, Selected timepoints from the timelapse series showing the two perpendicular lines used for the kymograph analysis. *c*, *bottom panels,* Kymograph of MyoIIA cluster coalescence in a walking cell. A line perpendicular (latitudinal) or parallel (longitudinal) to the direction of cell migration was drawn across the length of the cell and the intensities of MyoIIA-GFP (green) and actin-mCherry (red) were measured along these lines during crawling. MyoIIA cluster streaks are highlighted with white lines on the overlay panels. *d*, Kimograph analysis of MyoIIA clusters in a sliding cell; represented and analyzed as in *c*.

and functioning cooperatively but rather that they may be individually moving along predefined tracks, likely actin itself.

MyoIIA cluster movement was also identifiable in sliding cells although these clusters generally remained more diffuse throughout the contact zone (relative to actin-mCherry) and did not move inward from the sides to the same extent as in walking cells (Fig. 6, *b* and *d*, *bottom panels*, and supplemental movie 8). In addition, during sliding motility, MyoIIA clusters only rarely moved against the general direction of cell motion. In these cases, the inward movement of a cluster was often associated with, or closely followed, turns in the migration path and may represent a "tuning" of directionality through MyoIIA. An example of this is shown as the streak of MyoIIA-GFP fluorescence at the front of the leading edge in the kymograph in Fig. 5*c* (at the 200 s timepoint) and in Fig. 6*b* (*bottom panel*, white arrowheads). The speed of MyoIIA cluster movement in both crawling modes was nearly the same ($\cong$0.11 μm/sec) and was similar in magnitude to MyoIIA movement along actin.

MyoIIA and substrate adhesion strength regulate T cell adhesion surface

To gain further insight on how T cell scanning behavior may be regulated, we then analyzed how the interplay of MyoIIA function and substrate adhesion strength could regulate T cell contact area. When T cells were plated on "blocked" surfaces, lacking specific adhesion molecules, MyoIIA depletion resulted in a 2.6-fold average increase of the total surface contact area of D10 T cells measured using actin-GFP fluorescence detected in the TIRF field (Fig. 7, *a* and *b*). Given that the predominant T cell integrins have little to no affinity for this surface, it is most likely that the increased spreading resulted from a general loss of cortical tension. This was supported by comparing this spreading with that of cells plated on high concentration of integrin ligands (ICAM-1). On this high affinity substrate, MyoIIA competent cells increased spreading an average of 1.6-fold relative to the low affinity substrate, showing that integrin affinity could encourage contact. However,

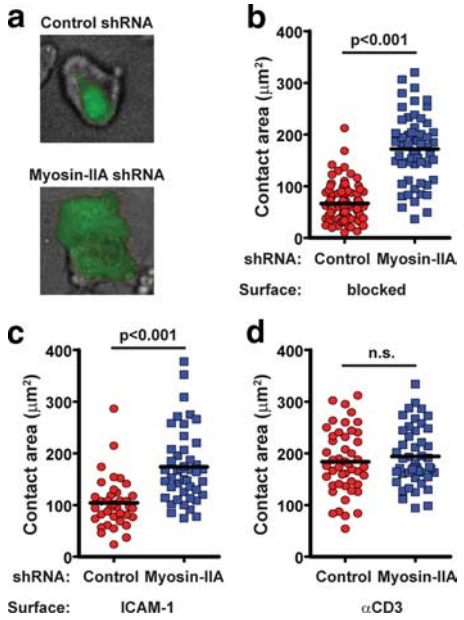

FIGURE 7. MyoIIA regulates T cell adhesion area. Measurement of substrate contact area of T cells by TIRF microscopy. Cells were transfected and imaged as described in Fig. 2. *a*, Representative cells from control- or MyoIIA-shRNA treated cells plated on blocked surfaces are shown. The brightfield images are overlaid with the TIRF actin-GFP fluorescence (in green). Cells are equivalently scaled. *b*, Contact area of cells plated overnight in blocked chamberslides. *c*, Contact area of cells plated overnight in ICAM-1 coated chamberslides. *d*, Contact area of cells plated for 1 h on anti-CD3 coated chamberslides. Results are pooled from three independent experiments.

MyoIIA depletion augmented this an additional 1.7-fold and essentially to the same degree achieved when integrins were not present (Fig. 7*c*). This suggests a critical role for cortical tension and MyoIIA activity in particular in regulating the size of adhesions. Our data is in accordance with the finding that MyoIIA-generated force regulates cell spreading in fibroblasts (29).

Notably, TCR signaling in response to immobilized Abs to CD3 resulted in a contact zone that was equivalent to that observed in MyoIIA-depleted cells with or without TCR engagement (Fig. 7, *b–d*). This result is consistent with our previous finding that TCR engagement leads to MyoIIA H chain phosphorylation (24) and thus inactivation of this myosin motor (30, 31). Overall, our data shows that MyoIIA regulates, in concert with adhesion forces, the overall size of amoeboid cell adhesions.

MyoIIA regulates T cell crawling within a three-dimensional environment

Finally, given that T cells typically migrate through a fibrous three-dimensional network in vivo, we analyzed T cell migration within collagen lattices of varying densities to characterize the effects of MyoIIA inhibition on motility in a three-dimensional environment. This analysis demonstrated that at low (0.75 mg/ml) and intermediate (1.5 mg/ml) collagen concentrations at least 80% of T cells are motile (Fig. 8*a*), with average migration rates of 8.3 μm/min and 10.3 μm/min, respectively. At these collagen concentrations, MyoIIA inhibition with blebbistatin resulted in a 47% average reduction in the percentage of motile cells (Fig. 8*a*) and a ~50% reduction in the speed of the motile population. This suggested that, with complete myosin blockade, T cells in low-density substrate environments do not strictly require MyoIIA for their motility, most likely using actin polymerization-based motility mechanisms. T cells in higher collagen concentration lattices (3 mg/ml) had a slightly reduced fraction of motile cells and migration rate in the absence of MyoIIA blockade. However, upon MyoIIA inhibition, the dependency of T cell migration on MyoIIA function in the dense lattice was much more pronounced with a 78% reduction in the percentage of motile cells (Fig. 8*a*) and with average velocities of the motile population of just 3.1 μm/min. Overall, this suggested a more stringent requirement for MyoIIA for motility within a more dense or constrictive local environment and that T cells can use MyoIIA-independent motility mechanisms when the local environment is more "permissive". Analysis of T cell displacement over the square-root of time in the collagen lattices confirmed the loss of "fast" moving cells following MyoIIA inhibition (Fig. 8*b*), supporting the importance of MyoIIA activity to achieve fast migration rates in a three-dimensional environment.

Discussion

In this study, we provide evidence for a MyoIIA-dependent unique discontinuous mode of motility in amoeboid lymphocytes in which adhesion zones influence one another across relatively short distances but coordinate to drive rapid cellular translocation. In addition, we show that upon MyoIIA inhibition, or in the presence of high adhesion substrates, T cells switch to a motility mode with a single contact zone to the substrate, which resembles "mesenchimal" fibroblast crawling. Hogg and colleagues (32) have described an adhesive structure, which they term "focal zone", enriched in high affinity LFA-1 and talin localized at the mid-cell area of T cells crawling on ICAM-1 on lipid bilayers. Although the dynamics of this contact zone are similar to what we have observed in sliding cells (detected in T cells crawling on ICAM-1 or following

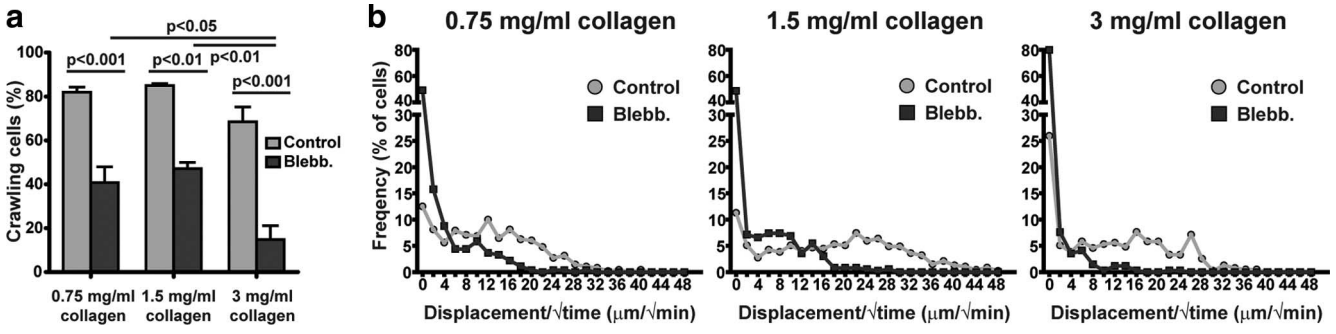

FIGURE 8. MyoIIA regulates T cell crawling within a three-dimensional environment. *a*, Activated primary DO.11.10 T cells were embedded in collagen lattices of varying density (as indicated) in the presence or absence of the myosin-II inhibitor blebbistatin. Cells were imaged for 30 min. and the fraction of motile cells was then measured. *b*, Analysis of the frequency distribution of the displacement over the square-root of time of control or blebbistatin treated primary T cells embedded in collagen lattices of various densities. Results shown are from three independent experiments.

MyoIIA depletion), the crawling speed is similar to what we observe in walking cells. This difference in the correlation between motility mode and speed may be due to the fact that in their experimental system ICAM-1 is freely diffusible on the lipid bilayer, while in our system ICAM-1 is immobilized on the substrate. Other experimental differences such as the source of T cells and the use of Mg^{2+} to induce a high affinity state of LFA-1 by Hogg and colleagues may also account for the observed differences.

Unlike sliding motility, we show that fast amoeboid motility is dependent on MyoIIA compressions, within rearward contact zones, that propel the cell forward and likely facilitate the formation of new adhesions at the front. Our findings therefore support a mechanism by which MyoIIA pushes the cell forward through contractions at the rear and mid-body rather than pulling the cell forward from the front, as is mostly the case for highly adherent cells such as fibroblast and epithelial cells. In support of this, contractile stresses in neutrophils and forces in *Dictyostelium* are mainly concentrated at the rear of the cell to facilitate pushing the cell forward and retraction of the rear (33, 34). Overall, rear-based force generation might be possible, at least in part, due to the small size of these cell types. At lengths of 5–15 μm, myosin-II-dependent compression forces (35) would tend to propagate across the entire cytoplasm very rapidly and, unlike larger cells, may permit distal transmission of pressure gradients from one adhesion zone at the back of the cell to regions of membrane at the front.

According to the adhesion-dependent ("haptokinetic") migration model, cells have maximal migration rates at intermediate adhesion strengths (36, 37). In epithelial cell migration this likely occurs via an interplay between adhesion, regulated by focal adhesion dynamics, and contraction forces mediated by the actomyosin cytoskeleton (14). In contrast to strict haptokinetic migration, dual modes of motility (i.e., haptokinetic-sliding vs amoeboid-walking) have potential advantages for in vivo lymphocyte migration within varying environments. A fast amoeboid migratory method using weak adhesions would permit cells to traverse tissues by virtue of a collection of relatively weak interactions and cell-autonomous shape deformations rather than requiring specific stronger adhesion surfaces to be present. Such is consistent with data showing a relative insensitivity of T cell migration to the absence of LFA-1-ICAM-1 interactions in lymph nodes (38), or upon blockade of β1, β2, or β3 integrins in collagen matrices (39). Furthermore, for amoeboid cells in a complex three-dimensional environment, the surrounding lattice itself may prove particularly suited for a cell to push against in the absence of distinct molecular adhesions. Recent findings on dendritic cell motility in the absence of integrin expression support the concept of adhesion-independent migration in three-dimensional environments and in vivo (40). These authors also show that MyoIIA function in dendritic cells is specifically required to provide the contractile force needed to squeeze through narrow gaps during crawling within dense three-dimensional environments (40). Our results on T cell crawling in collagen matrices in the presence of MyoIIA inhibition as well as our data indicating that MyoIIA contractions at the rear and mid-body play a role in pushing T cells forward are consistent with their findings.

In contrast, encounter with cues leading to MyoIIA inactivation, such as those generating calcium transients (41) and notably TCR signaling, could result in increased surface contact and reduced speeds (24, 42). In the context of T cells scanning APCs in search of cognate Ag, the effects of MyoIIA inhibition could increase the ability to sense sparsely distributed antigenic signals and be a factor leading to full T cell activation and immune responses.

Overall, our data suggests that T cells exhibit two distinct crawling modes that differ in their speed and surface scanning potential and that MyoIIA activity in concert with substrate adhesion strength regulate the transition between these two modes.

Acknowledgments

We thank S. Jiang and C. McArthur for expert technical assistance with cell sorting and A. Bullen for assistance in maintenance of microscopes. We thank O. Weiner for supplying HL-60 cells. We thank H. Bourne, O. Weiner, and R. Friedman (University of California, San Francisco, CA) for critical reading of the manuscript.

Disclosures

The authors have no financial conflict of interest.

References

1. Horwitz, R., and D. Webb. 2003. Cell migration. *Curr. Biol.* 13: R756–759.
2. Ridley, A. J., M. A. Schwartz, K. Burridge, R. A. Firtel, M. H. Ginsberg, G. Borisy, J. T. Parsons, and A. R. Horwitz. 2003. Cell migration: integrating signals from front to back. *Science* 302: 1704–1709.
3. Pollard, T. D., and G. G. Borisy. 2003. Cellular motility driven by assembly and disassembly of actin filaments. *Cell* 112: 453–465.
4. Friedl, P., S. Borgmann, and E. B. Brocker. 2001. Amoeboid leukocyte crawling through extracellular matrix: lessons from the *Dictyostelium* paradigm of cell movement. *J. Leukocyte Biol.* 70: 491–509.
5. Sanchez-Madrid, F., and M. A. del Pozo. 1999. Leukocyte polarization in cell migration and immune interactions. *EMBO J.* 18: 501–511.
6. Wolf, K., R. Muller, S. Borgmann, E. B. Brocker, and P. Friedl. 2003. Amoeboid shape change and contact guidance: T-lymphocyte crawling through fibrillar collagen is independent of matrix remodeling by MMPs and other proteases. *Blood* 102: 3262–3269.
7. Bajenoff, M., J. G. Egen, L. Y. Koo, J. P. Laugier, F. Brau, N. Glaichenhaus, and R. N. Germain. 2006. Stromal cell networks regulate lymphocyte entry, migration, and territoriality in lymph nodes. *Immunity* 25: 989–1001.
8. von Andrian, U. H., and C. R. Mackay. 2000. T-cell function and migration: two sides of the same coin. *N. Engl. J. Med.* 343: 1020–1034.
9. Wolf, K., I. Mazo, H. Leung, K. Engelke, U. H. von Andrian, E. I. Deryugina, A. Y. Strongin, E. B. Brocker, and P. Friedl. 2003. Compensation mechanism in tumor cell migration: mesenchymal-amoeboid transition after blocking of pericellular proteolysis. *J. Cell Biol.* 160: 267–277.
10. Wyckoff, J. B., S. E. Pinner, S. Gschmeissner, J. S. Condeelis, and E. Sahai. 2006. ROCK- and myosin-dependent matrix deformation enables protease-independent tumor-cell invasion in vivo. *Curr. Biol.* 16: 1515–1523.
11. Weber, I., E. Wallraff, R. Albrecht, and G. Gerisch. 1995. Motility and substratum adhesion of *Dictyostelium* wild-type and cytoskeletal mutant cells: a study by RICM/bright-field double-view image analysis. *J. Cell Sci.* 108: 1519–1530.
12. Murray, J., H. Vawter-Hugart, E. Voss, and D. R. Soll. 1992. Three-dimensional motility cycle in leukocytes. *Cell Motil. Cytoskeleton* 22: 211–223.
13. Dustin, M. L. 2004. Stop and go traffic to tune T cell responses. *Immunity* 21: 305–314.
14. Gupton, S. L., and C. M. Waterman-Storer. 2006. Spatiotemporal feedback between actomyosin and focal-adhesion systems optimizes rapid cell migration. *Cell* 125: 1361–1374.
15. Kolega, J. 2006. The role of myosin II motor activity in distributing myosin asymmetrically and coupling protrusive activity to cell translocation. *Mol. Biol. Cell* 17: 4435–4445.
16. Even-Ram, S., A. D. Doyle, M. A. Conti, K. Matsumoto, R. S. Adelstein, and K. M. Yamada. 2007. Myosin IIA regulates cell motility and actomyosin-microtubule crosstalk. *Nat. Cell Biol.* 9: 299–309.
17. Sandquist, J. C., K. I. Swenson, K. A. Demali, K. Burridge, and A. R. Means. 2006. Rho kinase differentially regulates phosphorylation of nonmuscle myosin II isoforms A and B during cell rounding and migration. *J. Biol. Chem.* 281: 35873–35883.
18. Wessels, D., D. R. Soll, D. Knecht, W. F. Loomis, A. De Lozanne, and J. Spudich. 1988. Cell motility and chemotaxis in *Dictyostelium* amebae lacking myosin heavy chain. *Dev. Biol.* 128: 164–177.
19. Laevsky, G., and D. A. Knecht. 2003. Cross-linking of actin filaments by myosin II is a major contributor to cortical integrity and cell motility in restrictive environments. *J. Cell Sci.* 116: 3761–3770.
20. Smith, A., M. Bracke, B. Leitinger, J. C. Porter, and N. Hogg. 2003. LFA-1-induced T cell migration on ICAM-1 involves regulation of MLCK-mediated attachment and ROCK-dependent detachment. *J. Cell Sci.* 116: 3123–3133.
21. Morin, N. A., P. W. Oakes, Y. M. Hyun, D. Lee, E. Y. Chin, M. R. King, T. A. Springer, M. Shimaoka, J. X. Tang, J. S. Reichner, and M. Kim. 2008. Nonmuscle myosin heavy chain IIA mediates integrin LFA-1 de-adhesionduring T lymphocyte migration. *J. Exp. Med.* 205: 195–205.
22. Pasternak, C., J. A. Spudich, and E. L. Elson. 1989. Capping of surface receptors and concomitant cortical tension are generated by conventional myosin. *Nature* 341: 549–551.
23. Jeon, T. J., D. J. Lee, S. Merlot, G. Weeks, and R. A. Firtel. 2007. Rap1 controls cell adhesion and cell motility through the regulation of myosin II. *J. Cell Biol.* 176: 1021–1033.
24. Jacobelli, J., S. A. Chmura, D. B. Buxton, M. M. Davis, and M. F. Krummel. 2004. A single class II myosin modulates T cell motility and stopping, but not synapse formation. *Nat. Immunol.* 5: 531–538.

25. Kolega, J. 2004. Phototoxicity and photoinactivation of blebbistatin in UV and visible light. *Biochem. Biophys. Res. Commun.* 320: 1020–1025.
26. Straight, A. F., A. Cheung, J. Limouze, I. Chen, N. J. Westwood, J. R. Sellers, and T. J. Mitchison. 2003. Dissecting temporal and spatial control of cytokinesis with a myosin II Inhibitor. *Science* 299: 1743–1747.
27. Jay, P. Y., P. A. Pham, S. A. Wong, and E. L. Elson. 1995. A mechanical function of myosin II in cell motility. *J. Cell Sci.* 108: 387–393.
28. Ponti, A., A. Matov, M. Adams, S. Gupton, C. M. Waterman-Storer, and G. Danuser. 2005. Periodic patterns of actin turnover in lamellipodia and lamellae of migrating epithelial cells analyzed by quantitative Fluorescent Speckle Microscopy. *Biophys. J.* 89: 3456–3469.
29. Cai, Y., N. Biais, G. Giannone, M. Tanase, G. Jiang, J. M. Hofman, C. H. Wiggins, P. Silberzan, A. Buguin, B. Ladoux, and M. P. Sheetz. 2006. Nonmuscle myosin IIA-dependent force inhibits cell spreading and drives F-actin flow. *Biophys J.* 91: 3907–3920.
30. Dulyaninova, N. G., V. N. Malashkevich, S. C. Almo, and A. R. Bresnick. 2005. Regulation of myosin-IIA assembly and Mts1 binding by heavy chain phosphorylation. *Biochemistry* 44: 6867–6876.
31. Bresnick, A. R. 1999. Molecular mechanisms of nonmuscle myosin-II regulation. *Curr. Opin. Cell Biol.* 11: 26–33.
32. Smith, A., Y. R. Carrasco, P. Stanley, N. Kieffer, F. D. Batista, and N. Hogg. 2005. A talin-dependent LFA-1 focal zone is formed by rapidly migrating T lymphocytes. *J. Cell Biol.* 170: 141–151.
33. Smith, L. A., H. Aranda-Espinoza, J. B. Haun, M. Dembo, and D. A. Hammer. 2007. Neutrophil traction stresses are concentrated in the uropod during migration. *Biophys. J.* 92: L58–L60.
34. Uchida, K. S., T. Kitanishi-Yumura, and S. Yumura. 2003. Myosin II contributes to the posterior contraction and the anterior extension during the retraction phase in migrating *Dictyostelium* cells. *J. Cell Sci.* 116: 51–60.
35. Charras, G. T., J. C. Yarrow, M. A. Horton, L. Mahadevan, and T. J. Mitchison. 2005. Non-equilibration of hydrostatic pressure in blebbing cells. *Nature* 435: 365–369.
36. DiMilla, P. A., K. Barbee, and D. A. Lauffenburger. 1991. Mathematical model for the effects of adhesion and mechanics on cell migration speed. *Biophys. J.* 60: 15–37.
37. Palecek, S. P., J. C. Loftus, M. H. Ginsberg, D. A. Lauffenburger, and A. F. Horwitz. 1997. Integrin-ligand binding properties govern cell migration speed through cell-substratum adhesiveness. *Nature* 385: 537–540.
38. Woolf, E., I. Grigorova, A. Sagiv, V. Grabovsky, S. W. Feigelson, Z. Shulman, T. Hartmann, M. Sixt, J. G. Cyster, and R. Alon. 2007. Lymph node chemokines promote sustained T lymphocyte motility without triggering stable integrin adhesiveness in the absence of shear forces. *Nat. Immunol.* 8: 1076–1085.
39. Friedl, P., F. Entschladen, C. Conrad, B. Niggemann, and K. S. Zanker. 1998. $CD4^+$ T lymphocytes migrating in three-dimensional collagen lattices lack focal adhesions and utilize β1 integrin-independent strategies for polarization, interaction with collagen fibers and locomotion. *Eur. J. Immunol.* 28: 2331–2343.
40. Lammermann, T., B. L. Bader, S. J. Monkley, T. Worbs, R. Wedlich-Soldner, K. Hirsch, M. Keller, R. Forster, D. R. Critchley, R. Fassler, and M. Sixt. 2008. Rapid leukocyte migration by integrin-independent flowing and squeezing. *Nature* 453: 51–55.
41. Negulescu, P. A., T. B. Krasieva, A. Khan, H. H. Kerschbaum, and M. D. Cahalan. 1996. Polarity of T cell shape, motility, and sensitivity to antigen. *Immunity* 4: 421–430.
42. Dustin, M. L., S. K. Bromley, Z. Kan, D. A. Peterson, and E. R. Unanue. 1997. Antigen receptor engagement delivers a stop signal to migrating T lymphocytes. *Proc. Natl. Acad. Sci. USA* 94: 3909–3913.